AIAA'87

AIAA-87-2165

Test Flow Calibration Study of the Langley Arc-Heated Scramjet Test Facility

Scott R. Thomas, Randall T. Voland and Robert W. Guy, NASA Langley Research Center, Hampton, VA

AIAA/SAE/ASME/ASEE 23rd Joint Propulsion Conference

June 29-July 2, 1987/San Diego, California

TEST FLOW CALIBRATION STUDY OF THE LANGLEY ARC-HEATED SCRAMJET TEST FACILITY

Scott R. Thomas[†], Randall T. Voland[††], and Robert W. Guy[†††]
Langley Research Center
Hampton, Virginia

Abstract

An experimental research program to define the test flow at the exits of two square cross-section, contoured facility nozzles with nominal exit Mach numbers of 4.7 and 6 is described. This study provided detailed calibration data for the NASA-Langley Arc-Heated Scramjet Test Facility over a range of simulated flight conditions from Mach 5.5 (at altitudes from 98,600 to 128,000 ft.) to Mach 7 (at altitudes from 108,000 to 149,000 ft.). Distributions of pitot pressure, static pressure, and total temperature were measured at the nozzle exits over this range of test conditions. These distributions of thermodynamic properties were used to calculate the distributions of test flow Mach number and mass flow at the nozzle exits. Contour maps of the thermodynamic properties and the calculated quantities are presented, and an assessment is made of flow quality of square cross-section, contoured nozzles over a nozzle exit Mach number range from 3.5 to 6 (simulated flight Mach numbers from 4 to 7). Facility total mass flow, obtained by integration of the nozzle exit mass flow contours, compared favorably to measured facility total mass flow. The contour maps were also used to determine the mass flow approaching the inlets of various scramjet engines.

Nomenclature

CR	Scramjet engine contraction ratio; engine projected geometric capture area relative to engine minimum cross section area
H	Facility nozzle exit dimension (height and width)
$h_{t,1}$	Test flow total enthalpy in the facility plenum chamber
$h_{t,\infty}$	Total enthalpy corresponding to the simulated free stream flight condition
$\dot{m}_{engine}$	Portion of facility test flow which passes through the projected scramjet geometric capture area
$\dot{m}_{total}$	Total facility mass flow rate
M_1	Mach number at the nozzle exit simulating scramjet inlet Mach number
M_∞	Simulated free stream flight Mach number
p_1	Static pressure at the nozzle exit
$p_{t,1}$	Test flow total pressure in the facility plenum chamber
$p_{t,2}$	Measured pitot pressure at the exit of the facility contoured nozzle
R	Specific gas constant
Re_1	Reynolds number per foot
T_1	Static temperature at the nozzle exit
T_{core}	The mean value of all total temperature measurements obtained at locations more than 2.5 inches from the nozzle wall for a given test condition
$T_{t,1}$	Test flow total temperature in the facility plenum chamber
$T_{t,2}$	Measured total temperature at the exit of the facility contoured nozzle
U_1	Flow velocity at the nozzle exit
W	Width of scramjet engine
Y	Vertical nozzle coordinate
γ	Ratio of specific heats
ρ_1	Static density at the nozzle exit

Introduction

Development of airframe-integerated scramjet (supersonic combustion ramjet) technology continues to progress at NASA's Langley Research Center. The scramjet program focus is a fixed-geometry, hydrogen-burning, advanced engine concept (Fig. 1) that has been shown to potentially be a very efficient propulsion device at flight speeds above Mach 4.[1,2] The integrated design uses the underside of the flight vehicle as part of the propulsion system; i.e., the forebody provides aerodynamic precompression of the flow entering the inlet, and the aft portion of the vehicle is used as part of the nozzle expansion surface.

Experimental work in support of this scramjet concept includes inlet configuration tests, direct-connect combustor tests, and subscale engine tests. Inlet tests have been conducted in several Langley aerodynamic facilities,[3,4] while the direct-connect combustor tests have been conducted in a vitiated air (hydrogen-combustion-heated with oxygen replenishment) facility at Langley (for example, see Refs. 5 and 6). Scramjet engine tests at a simulated flight Mach number of 4 have been conducted in combustion-heated air facilities at the General Applied Science Laboratories (GASL) and at Langley.[7,8] Engine tests at a simulated flight Mach number of 7 have been conducted in the GASL facility and in electric-arc-heated air at the Langley Arc-Heated Scramjet Test Facility (AHSTF).[9] Those tests served to demonstrate the performance potential of the airframe-integrated scramjet engine concept, to indicate areas of engine operation requiring further research, and to define facility improvements which would enhance future scramjet related research.

The engine test facilities are different from most aerodynamic wind tunnels because the total

[†]Research Scientist, Hypersonic Propulsion Branch, High-Speed Aerodynamics Division
[††]Research Scientist, Hypersonic Propulsion Branch, High-Speed Aerodynamics Division, Member AIAA
[†††]Senior Research Scientist, Hypersonic Propulsion Branch, High-Speed Aerodynamics Division

enthalpy corresponding to the flight Mach number is duplicated, and tests are conducted at total pressures corresponding to practical flight altitudes. In addition, engine-airframe integration effects such as vehicle bow shock precompression and boundary layer ingestion by the scramjet are simulated. To accomplish this, the scramjet is mounted in the facility as shown in Figure 2. The flight vehicle bow shock precompression is simulated by testing at a tunnel Mach number less than the Mach number which corresponds to the tunnel flow total enthalpy. Flight vehicle boundary layer ingestion is partially simulated by mounting the scramjet model so that the facility nozzle boundary layer approaching the model top surface is ingested.

The Langley Arc-Heated Scramjet Test Facility has typically been referred to in previous literature as the Mach 7 Scramjet Test Facility. However, the effort of References 10 and 11 expanded the test capability to a range of Mach numbers (from Mach 4.7 to Mach 7); therefore, the early facility designation is no longer accurate and implies a limitation (i.e., Mach 7 testing only) which is no longer true. With the proper facility contoured nozzles, a complete test program over a range of Mach numbers could be accomplished without removing the model from the test section. Therefore, two new facility contoured nozzles, with nominal exit Mach numbers of 6 and 4.7, were designed and constructed. Both nozzles had square cross-sections at all axial locations. This square cross-section design minimized surface area for heat losses in the throat region and, compared to a rectangular throat, reduced the effect of (and errors due to) the boundary layer growth in the throat region.

The present study was conducted to calibrate (i.e., define test flow thermodynamic conditions) at the exits of the new Mach 6 and the Mach 4.7 nozzles. It was necessary to obtain a detailed nozzle flow calibration because scramjet engine performance is based on the properties of the test flow entering the inlet, and if these properties are well defined, performance can be more accurately determined. Note that the existence of a boundary layer in the test flow is desirable for tests of airframe-integrated scramjets because this allows some simulation of the vehicle forebody boundary layer as outlined in Reference 1.

This report documents the calibration of both the Mach 6 and Mach 4.7 nozzles. Nozzle exit contour maps of measured thermodynamic properties, calculated Mach number, and calculated mass flow are presented. The contour maps are used to determine the mass flow approaching the inlets of various scramjet engines.

The Langley Arc-Heated Scramjet Test Facility

The various components of the Langley Arc-Heated Scramjet Test Facility tunnel circuit are shown in Figure 3 and the facility is described in detail in Reference 12. The primary purpose of the facility is to provide a test flow with true velocity, static temperature, and static pressure over a simulated flight Mach number range from 4.7 to 7, so that the performance of hydrogen-burning scramjet engines may be assessed.

A longitudinal section view of the electric arc heater and the plenum chamber is shown in Figure 4. The arc is established between the electrodes and, except for the termination regions, is confined along the heater centerline by the vortex flow of the main air stream, which is purposely injected with a tangential velocity (swirled in). The arc-heated air (total temperature approximately 8500°R) is mixed in the plenum chamber with an unheated bypass airstream to form a resultant test stream with the desired stagnation conditions (1000°R $< T_{t,1} <$ 4000°R; $P_{t,1} <$ 660 psia). The bypass air is injected radially from the plenum rings. This radial injection enhances mixing and also helps to break up the swirl downstream of the arc heater to improve flow quality for engine testing. This test gas mixture is expanded through a contoured nozzle into the test section. The flow is then diffused to subsonic velocity, cooled by an aftercooler, and exhausted into a vacuum sphere (Fig. 3).

Nozzle Calibration

Schematics of the Mach 6 and Mach 4.7 nozzles are presented in Figure 5. These nozzles have square cross-sections throughout; the exit plane of the Mach 6 nozzle is 10.89 inches by 10.89 inches and the exit plane of the Mach 4.7 nozzle is 11.174 inches by 11.174 inches. Nozzles of this type (where there is contouring on all four surfaces) have not been used in any previous tests at the AHSTF. Success in future engine tests dictates a thorough knowledge of flow conditions at the exits of these facility nozzles. This flow definition required detailed measurements of pitot pressure, static pressure, and total temperature so that Mach number and mass flow per unit area could be calculated and flow uniformity assessed.

Instrumentation

Rake surveys at the exits of both facility contoured nozzles provided distributions of pitot pressure, static pressure, and total temperature. The survey probes used in this study are shown schematically in Figure 6. Both the pitot pressure probes and the static pressure probes were of standard design. Since none of the probes were water-cooled, the pitot probes used in the Mach 6 nozzle calibration were of larger diameter to withstand the higher heating rates. All probes were constructed from steel. Iridium versus Iridium/40 percent rhodium thermocouple probes were used for surveys of the Mach 6 nozzle at test conditions where the flow total temperature was near Mach 7 simulated conditions (approximately 4000°R). This probe was made of steel and also coated with zirconium oxide to survive the high temperature test conditions. Chromel-alumel thermocouple probes were used for all surveys of the Mach 4.7 nozzle. This probe design was sufficient to withstand test conditions up to simulated Mach 5.5 total temperatures (approximately 2700°R).

Measured and Calculated Data

During this test program, nozzle exit flow surveys were obtained for all of the test conditions listed in Table 1. The contour maps of the resultant measured properties and calculated flow

parameters are very similar for all test conditions explored for each nozzle. Therefore, contours will only be presented here for the nominal test condition for each nozzle. The nominal test conditions are defined for the precompression ($M_1 < M_\infty$) shown in Table 1 at the lowest altitude simulation capability of the facility. For the Mach 6 nozzle, this corresponds to a total enthalpy of 1077 BTU/lbm (calculated using a facility energy balance as described in Ref. 12) and a facility total pressure of 584 psia. For the Mach 4.7 nozzle, this corresponds to a total enthalpy of 690 BTU/lbm and a facility total pressure of 177 psia.

Measurements of pitot pressure, total temperature, and static pressure were obtained with the Mach 4.7 nozzle at the nominal test condition. Measurements of pitot pressure and total temperature were obtained with the Mach 6 nozzle at the nominal test condition; however, instream static pressures were not measured at this condition because the uncooled probes would not have survived for the test time required for these measurements to settle near equilibrium conditions. Instead, ratios of static-to-total pressure measured at the exit of the Mach 6 nozzle at a facility total temperature of 1100°R and a total pressure of 325 psia were used to estimate the static pressure at the nominal Mach 6 condition. Wall static pressure axial distributions, which were measured at all test conditions, showed that the nozzle exit static pressure ratio at the nominal Mach 6 test condition (3960°R) was approximately 90 percent of the static pressure ratio measurements obtained at a total temperature of 1100°R. This factor was used to correct the static pressure data obtained at the lower total temperature to the nominal test condition.

Measurements of total temperature at the high temperatures and flow velocities involved in this test program are difficult to obtain with reasonable accuracy, since velocity, conduction, and radiation errors can be significant. The thermocouple temperature measurements were consistently lower than the total temperature predicted by a facility energy balance technique. Therefore the measurements were not used directly, but were assumed to provide a good indication of the total temperature distribution and thermal uniformity. The measurements of total temperature were normalized by the average core flow value (the core flow value is the mean of all measurements more than 2.5 inches from the nozzle wall). For both nominal test conditions, the core flow value was approximately 90 percent of the total temperature predicted by the facility energy balance.

The locations of data measurements of pitot pressure for the Mach 6 nozzle at the nominal condition is shown in Figure 7. This is typical of the data measurement distributions obtained for all measurements with each nozzle. As shown by this figure, more data was obtained in some regions of the nozzle then others; this sparcity of data could have yielded significant inaccuracy in evaluation of flow uniformity or subsequent calculations of flow properties. However, by design, the nozzles are symmetric around both the vertical and horizontal centerlines (actually any line passing through the nozzle centers). Profiles of data (both horizontal and vertical) at constant distance from the nozzle wall show good symmetry, which indicates that the nozzle flow is symmetric in all directions. Therefore, for analysis and flow evaluation during this study, the flow is assumed to be symmetrical around both the horizontal and vertical planes and the measured data were mirrored (reflected) around these centerlines. After mirroring, data were specified in the locations shown in Figure 7b. This allowed a much more complete and accurate analysis because distributions of flow properties were defined in regions where measured data were sparce. Using linear interpolation, evenly spaced data were obtained on a 45 by 45 point grid (approximately every 1/4 inch) for use in a contour plotting computer program.

The mirrored data were also used to calculate nozzle exit distributions of Mach number and mass flow. Pitot pressure and total temperature were determined at each calculation point by multiplying the pitot pressure ratio and total temperature ratio by the appropriate nominal facility stagnation condition (for the Mach 6 nozzle, $P_{t,1}$ = 584 psia and $T_{t,1}$ = 3965°R, for the Mach 4.7 nozzle, P_t = 177 psia and T_t = 2641°R). The static pressure at each point was determined by multiplying the static pressure ratio (corrected to the nominal test condition) by the nominal facility stagnation pressure.

For both nozzles the Mach number was calculated at each point using the local static pressure and pitot pressure in the Rayleigh - Pitot formula:

$$P_1/P_{t,2} = \left(\frac{5}{6M_1^2}\right)^{7/2} \left(\frac{7M_1^2 - 1}{6}\right)^{5/2}$$

The Mach number was calculated by iteration, since $P_1/P_{t,2}$ was the known quantity.

The calculation of unit mass flow rate for the nominal Mach 6 condition, where the total temperature was 3965°R, required modeling of a test flow in thermodynamic non-equilibrum. This was accomplished by developing a computer program which modeled vibrational non-equilibrum flow by incorporating a sudden freeze criteria as outlined in Reference 13 and 14, along with the equations of Reference 15 for molecular vibrational energy. The equation determined from this analysis that correlated mass flow as a function of local thermodynamic conditions near Mach 7 total enthalpy is:

$$\frac{\rho_1 U_1}{P_{t,2}} = \left(1.53 \times 10^{-4} + .000235\ (P_1/P_{t,2})\right) * \left(\frac{1100}{H_{t,1}}\right)$$

with ρ_1 in slugs/ft^3, U_1 in ft/sec, $P_{t,2}$ in lb$_f$/ft^2, P_1 in lb$_f$/ft^2, and $H_{t,1}$ in BTU/lb$_m$. This expression is a curve fit of the calculations made in this analysis which is considered to accurately predict the flow condition at the exit of the Mach 6 nozzle with Mach 7 total enthalpy.

Calculations of mass flow rate distribution for the Mach 4.7 nozzle were made with perfect gas assumptions using local values of static pressure, static temperature, and Mach number (as calculated

in the previous section) and the following equation:

$$\rho_1 U_1 = P_1 M_1 \left(\frac{\gamma}{RT_1}\right)^{1/2} \qquad \frac{\text{Slugs}}{\text{s-ft}^2}$$

where $\gamma = 1.4$
$R = 1716 \quad ft^2/s^2 {}^\circ R$

and ρ_1 is in slugs/ft^3, U_1 is in ft/s, P_1 is in lb_f/ft^2, and T_1 is in °R.

Nozzle Exit Flow Contours

Contour maps of measured data and calculated parameters are presented in Figure 8 for the Mach 6 nozzle and Figure 9 for the Mach 4.7 nozzle. All pitot and static pressure data are normalized by facility stagnation pressure (in the plenum chamber) and total temperature is normalized by the core value as explained earlier. These nozzle exit contours show lines of constant flow parameters. The numerical change in flow parameters is the same between each adjacent line (contour); therefore, a concentration of contours indicates a region of higher flow gradients. Significant gradients of all flow parameters exist across the exits of both nozzles. However, the gradients are more severe at the exit of the Mach 6 nozzle. This is emphasized by the centerline profiles of various flow parameters shown for the Mach 6 and Mach 4.7 nozzles in Figures 10 and 11, respectively. As indicated by the contour maps (Figs. 8 and 9), these centerline profiles involve the greatest degree of non-uniformity of any horizontal (or vertical) profile. In the Mach 6 nozzle, gradients exist almost 3 inches from the nozzle sidewalls. However, a uniform core is reached in the Mach 4.7 nozzle in less than half that distance.

Although the measured data and the respective contours and centerline profiles of flow properties indicate significant gradients in flow properties across the nozzle exits, the flow quality for the test conditions explored is considered to be of sufficient uniformity for subscale engine testing for two reasons. First, for airframe-integrated scramjet engine testing, an important part of simulation of a flight condition is ingestion of the non-uniform nozzle top surface air flow to simulate the ingestion of the non-uniform flow generated by the vehicle forebody which is an inherent part of the design. Therefore the existence of test flow non-uniformity is necessary, and, properly defining this flow (which was done in this study for all test conditions of interest) allows correct interpretation of the performance results. Second, all contours and centerline profiles of both measured and calculated parameters show that testing would be possible in essentially uniform flow if the engine was centered in the nozzle exit plane. Therefore, testing with and without ingestion of the nozzle top surface flow can be used to infer the relative importance of non-uniform flow in engine testing.

Mach number profiles at the nozzle centerline of the two nozzles tested during this study are compared with the Mach number distribution from a similar, square cross-section contoured nozzle (Ref. 16) with an exit Mach number of 3.5 ($T_{t,1}$ = 1630°R, $P_{t,1}$ = 92 psia) in Figure 12. This figure, along with comparison of Figures 10 and 11, indicates that the uniformity of flow parameters from these square cross-sectional nozzles may diminish with increasing nozzle exit Mach number. The distribution of flow parameters obtained in this calibration study could be to some extent facility-related or dependent on other parameters such as Reynolds number that vary between the test conditions; therefore, the differences may not be completely inherent in the nozzle design. Further definition and understanding of the flow quality from this type of nozzle should be pursued with computational fluid dynamics (CFD).

Mass Flow Rate Integration

The unit mass flow rate contours, Figures 8e and 9e, were integrated across the nozzle exit plane to determine total facility mass flow rate. These results for the nominal test conditions (and for all other cases shown in Table 1) are compared in Figure 13 with values of total facility mass flow rate as measured with ASME nozzles and turbine flowmeters. The agreement lends credence to the accuracy of the mass flow measurements at the exits of the nozzles.

In order to properly assess scramjet engine performance data, it is necessary to accurately determine the air mass flow that passes through the engine. This captured air mass flow is typically correlated as a product of two quantities. The first is the total mass flow that is approaching the engine (i.e. passes through the cross sectional plane defined by the height and width of the model). The second quantity is the percentage of that total mass flow (approaching the engine) that actually enters and passes through the engine, this quantity is referred to as the engine percent capture. The cross sectional dimensions of the current scramjet engine model (i.e., perpendicular to the test flow direction) are a height of 7.2 inches and width of 7.2 inches or less. The width of the current model is actually a variable and is a function of scramjet engine model contraction ratio (CR). The nominal location of the model relative to the nozzle exit plane is outlined in Figure 14 as a function of CR. During this study the flow properties (i.e., thermodynamic and calculated) were determined across the entire nozzle exit, including the region where the engine is located, and the percent of the total facility mass flow approaching the engine for each test case of interest was defined. Figure 15 specifies this mass flow approaching the engine as a function of the total facility mass flow for the nominal test conditions. These values are significantly higher (more than 15 percent) than the corresponding ratios of projected scramjet area to nozzle exit areas (for both nozzles) because of the higher mass flow rates near the center of each nozzle compared to near the walls. In addition to the mass flow approaching the engine, as shown in Figure 15, the engine percent capture is also needed to specify the actual mass flow through the engine for accurate correlation of performance data. The percent capture can be determined for an inlet configuration of interest either experimentally or computationally using the distribution of flow properties determined in this study as an upstream boundary condition. Determination of percent capture for various inlets was not a subject of the current study.

Concluding Remarks

This study provided a detailed test flow calibration of the NASA Langley Arc-Heated Scramjet Test Facility over a range of simulated flight conditions from Mach 5.5 (at altitudes from 98,600 to 128,000 ft.) to Mach 7 (at altitudes from 108,000 to 149,000 ft.). Specifically, the test flow was defined at the exit of two square cross-section, contoured facility nozzles with exit Mach numbers of 4.7 and 6. Distributions of pitot pressure, static pressure, and total temperature were measured for facility conditions of interest for testing of subscale scramjet engine models. These measurements were used to calculate corresponding distributions of Mach number and mass flow. Contour maps of measured and calculated properties were presented for nominal test conditions (lowest altitude simulation for each nozzle) as examples; these were representative of the results obtained for all test conditions. These distributions indicated that the flow uniformity is sufficient for scramjet engine testing and permitted the definition of Mach number and mass flow rate approaching scramjet inlets to enable accurate correlation and interpretation of subsequent test results.

References

1. Henry, John R. and Anderson, Griffin Y.: Design Considerations for the Airframe-Integrated Scramjet. NASA TM X-2895, 1973.

2. Jones, Robert A. and Huber, Paul W.: Airframe-Integrated Propulsion System for Hypersonic Cruise Vehicles. ICAS Proceedings 1978 - 11th Congress of the International Council of the Aeronautical Sciences (ICAS), Vol. 1 - Fuel Conservation, Hypersonic Vehicles, Environment Effects, Materials and Structures, Computational Aerodynamics, Wind Tunnels, Flight Testing, Stability and Control, J. Singer and R. Staufenbiel.

3. Trexler, Carl A. and Souders, Sue W.: Design and Performance at a Local Mach Number of 6 of an Inlet for an Integrated Scramjet Concept. NASA TN D-7944, August 1975.

4. Trexler, C. A.: Inlet Performance of the Integrated Langley Scramjet Module (Mach 2.3 to 7.6). Presented at the AIAA/SAE 11th Propulsion Conference, Anaheim, CA, September 1975.

5. McClinton, C. R. and Gooderum, P. B.: Direct-Connect Test of a Hydrogen-Fueled Three-Strut Injector for an Integrated Modular Scramjet Engine. Presented at the 14th JANNAF Combustion Meeting, Colorado Springs, CO, August 1977.

6. Northam, G. B.; Trexler, C. A.; and McClinton, C. R.: Flameholding Characteristics of a Swept-Strut H_2 Fuel-Injector for Scramjet Applications. Presented at the 17th JANNAF Combustion Meeting, Hampton, VA, September 1980.

7. Andrews, E. H.; Northam, G. B.; Torrence, M. G.; and Trexler, C. A.: Mach 4 Tests of a Hydrogen-Burning Airframe-Integrated Scramjet. Presented at the 18th JANNAF Combustion Meeting, Pasadena, CA, October 1981.

8. Guy, Robert W. and Mackley, Ernest A.: Initial Wind Tunnel Tests at Mach 4 and 7 of a Hydrogen-Burning, Airframe-Integreated Scramjet. NASA paper presented at the 4th International Symposium on Air Breathing Engines, Lake Buena Vista, FL, April 1979.

9. Guy, Robert W.; Torrence, Marvin G.; Mueller, James N.; and Sabol, Alexander P.: Initial Ground-Facility Tests at Mach 7 of a Hydrogen-Burning, Airframe-Integrated, Scramjet-Engine Model. NASA TM-84644, 1983.

10. Thomas, Scott R. and Guy, Robert W.: Expanded Operational Capabilities of the Langley Mach 7 Scramjet Test Facility. NASA TP-2186, 1983.

11. Thomas, Scott R. and Guy, Robert W.: Increased Capabilities of the Langley Mach 7 Scramjet Test Facility. AIAA/ASME/SAE 18th Joint Propulsion Conference, AIAA Paper No. 82-1240, June 21-23, 1982.

12. Guy, Robert W.; Torrence, Marvin G.; Sabol, Alexander R.; and Meuller, James N.: Operating Characteristics of the Langley Mach 7 Scramjet Test Facility. NASA TM-81929, 1981.

13. Guy, Robert W.: A Calibration and Diagnosis of the Test Stream of an Electric Arc-Heated Wind Tunnel. A Thesis presented to the faculty of the School of Engineering and Applied Science, University of Virginia, September 1969.

14. Lordi, J. A.; Mates, R. E.; and Moselle, J. R.: Computer Program for the Numerical Solution of Nonequilibrium Expansions of Reacting Gas Mixtures. CAL Report No. AD-1689-A-6, October 1965.

15. Erickson, Wayne D.: Vibrational-Nonequilibrium Flow of Nitrogen in Hypersonic Nozzles. NASA TN D-1810, June 1963.

16. Andrews, Earl H., Jr.: A Subsonic to Mach 5.5 Subscale Engine Test Facility. AIAA/SAE/ASME/ASEE 23rd Joint Propulsion Conference, AIAA Paper No. 87-2052, June 29-July 2, 1987.

17. National Advisory Committee for Aeronautics Equations, Tables, and Charts for Compressible Flow, Report 1135, 1953.

18. Winovich, Warren: On the Equilibrium Sonic Throat Method for Evaluating Electric-Arc Air-Heater Performance. NASA TN D-2132, 1964.

19. Phinney, R.: Nondimensional Solutions of Flows with Vibrational Relaxation. AIAA Journal, Vol. 2, No. 2, February 1964, pp. 240-244.

20. Blackman, V. H.: Vibrational Relaxation in O_2 and N_2. Journal Fluid Mechanics, Vol. 1, 1956, pp. 61-85.

Table 1: TEST CONDITIONS

MACH 6 NOZZLE

M_∞	Simulated Altitude (ft)	$h_{t,1}$ $\left(\frac{BTU}{lbm}\right)$	$T_{t,1}$ (°R)	$P_{t,1}$ (psia)	$\dot{m}_{total}$ (lbm/s)	R_e/ft
7	149,000	1232	4470	118	1.200	1.41×10^5
7	123,000	1138	4155	310	3.300	3.71×10^5
7*	108,000	1077	3965	584	6.330	7.0×10^5
--	--	264	1100	325	6.820	2.24×10^6

MACH 4.7 NOZZLE

M_∞	Simulated Altitude (ft)	$h_{t,1}$ $\left(\frac{BTU}{lbm}\right)$	$T_{t,1}$ (°R)	$P_{t,1}$ (psia)	$\dot{m}_{total}$ (lbm/s)	$R_{e,1}$/ft
5.5	128,000	755	2859	48	2.250	3.5×10^5
5.5	106,000	701	2679	125	5.93	8.5×10^5
5.5*	98,600	690	2641	177	8.460	1.15×10^6
--	--	264	1100	100	7.620	2.0×10^6

*Nominal Test Conditions

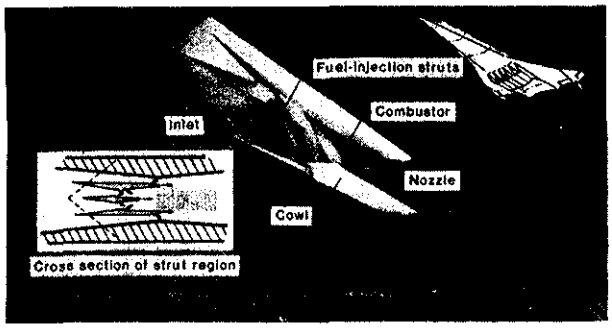

Fig. 1 - Airframe-integrated supersonic combustion ramjet.

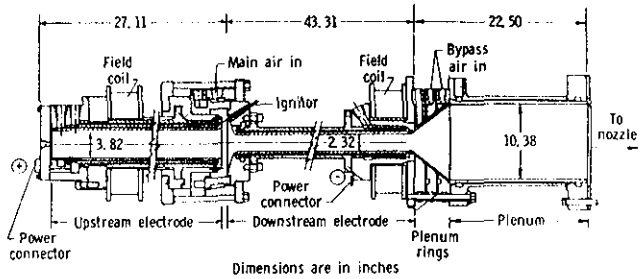

Fig. 4 - Section view of the arc heater and plenum chamber.

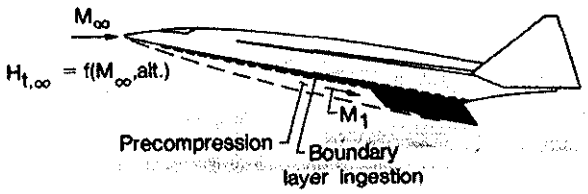

(a) Flight conditions.

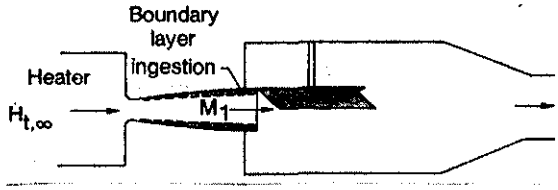

(b) Simulation in ground facility

Fig. 2 Simulation of flight conditions during scramjet engine testing.

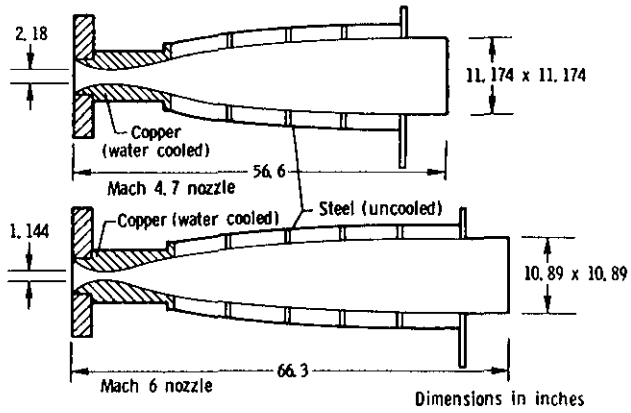

Fig. 5 - Schematics of square cross section facility contoured nozzles.

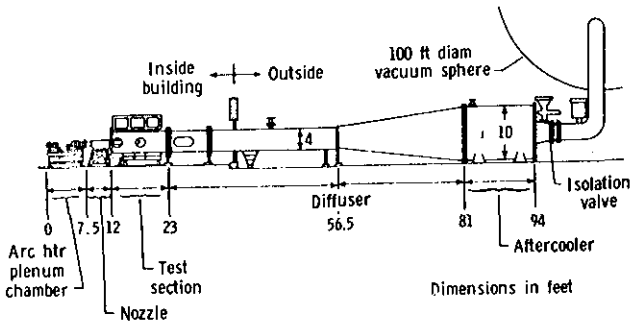

Fig. 3 - Elevation view of the Arc-Heated Scramjet Test Facility (AHSTF).

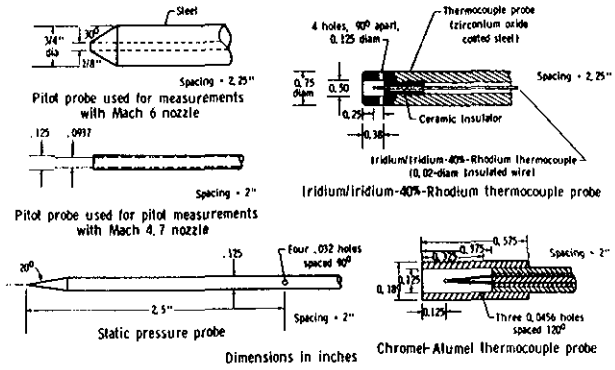

Fig. 6 - Flow measurement probes.

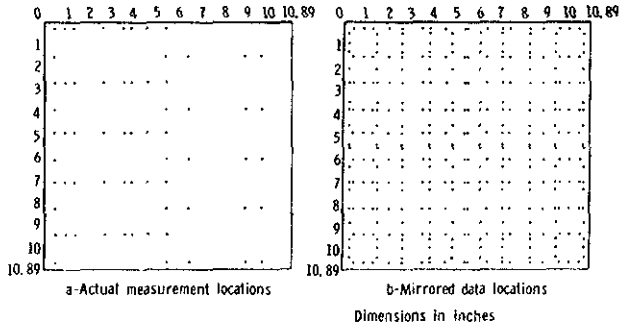

Fig. 7 - Actual and mirrored data measurement locations. (Pitot pressure measurements, Mach 6 nozzle, nominal conditions.)

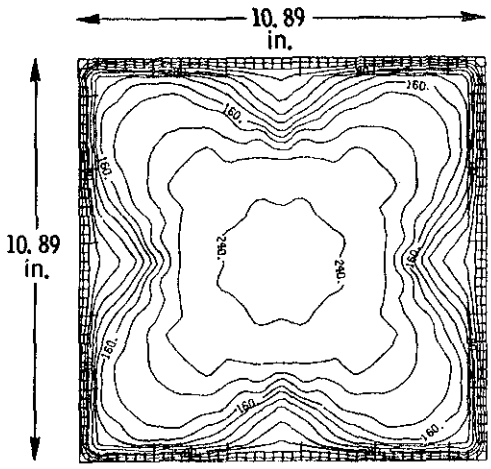

(a) Pitot pressure ratio. ($P_{t,2}/P_{t,1} \times 10^4$)

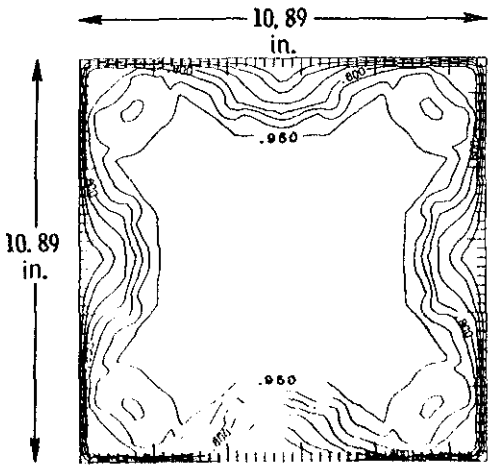

(b) Total temperature ratio. ($T_{t,2}/T_{core}$)

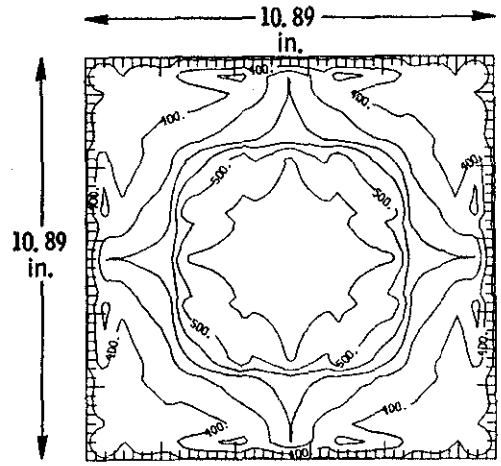

(c) Static pressure ratio. ($P_1/P_{t,1} \times 10^6$)

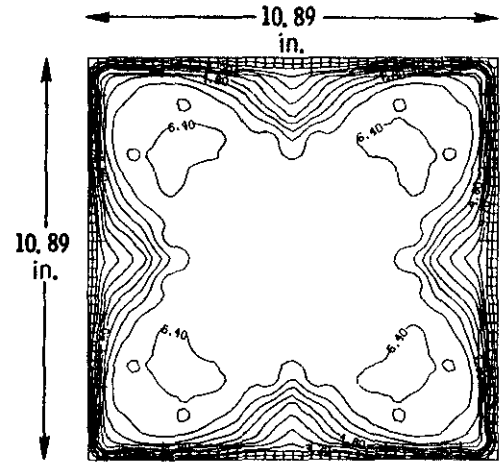

(d) Mach number.

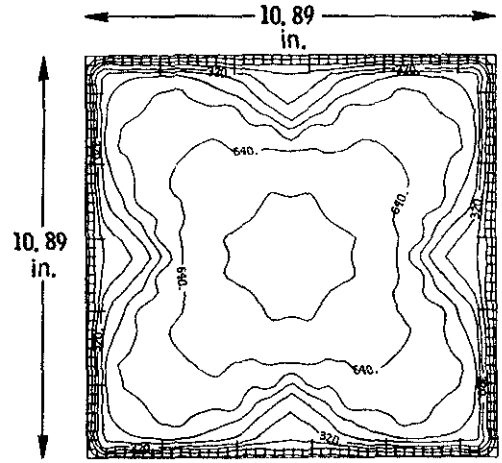

(e) Mass flow rate per unit area. ($lbm/s\ in^2 \times 10^4$)

Fig. 8 - Flow parameter contours at the exit of the Mach 6 nozzle.

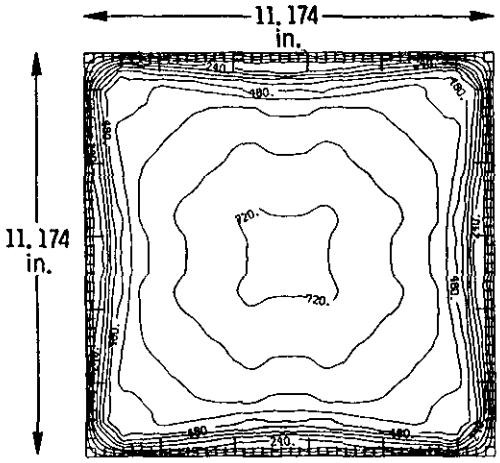

(a) Pitot pressure ratio.
($P_{t,2}/P_{t,1} \times 10^4$)

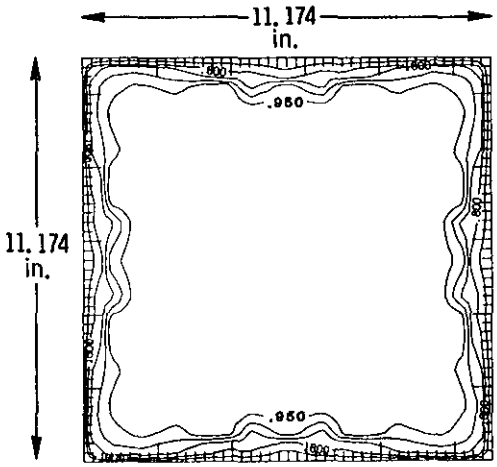

(b) Total temperature ratio.
($T_{t,2}/T_{core}$)

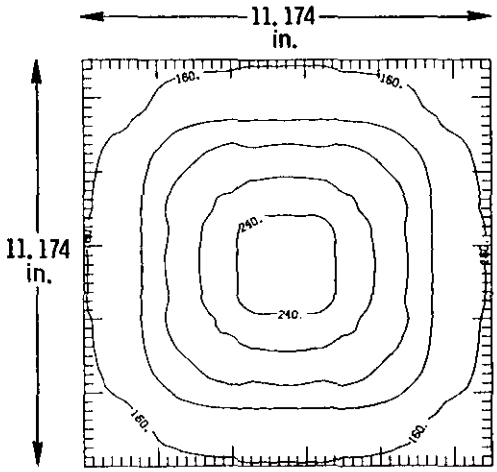

(c) Static pressure ratio.
($P_1/P_{t,1} \times 10^5$)

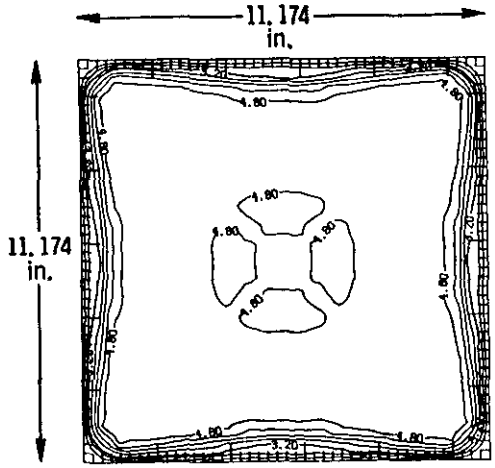

(d) Mach number.

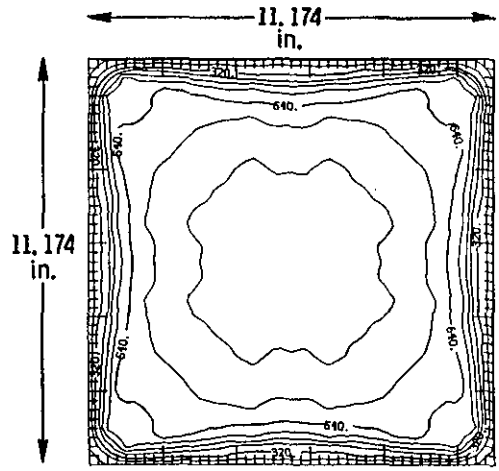

(e) Mass flow rate per unit area.
($lbm/s\ in^2 \times 10^4$)

Fig. 9 - Flow parameter contours at the exit of the Mach 4.7 nozzle.

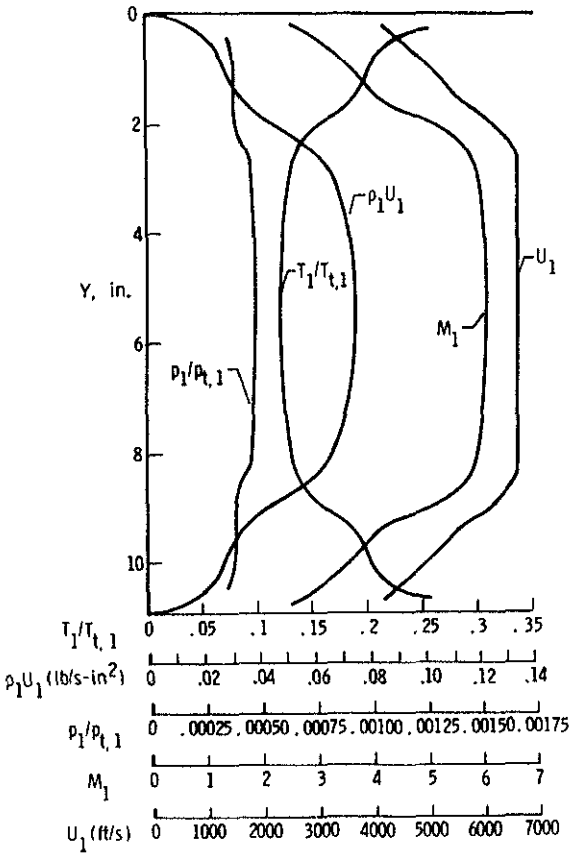

Fig. 10 - Centerline profiles of flow parameters for the Mach 6 nozzle (nominal test condition).

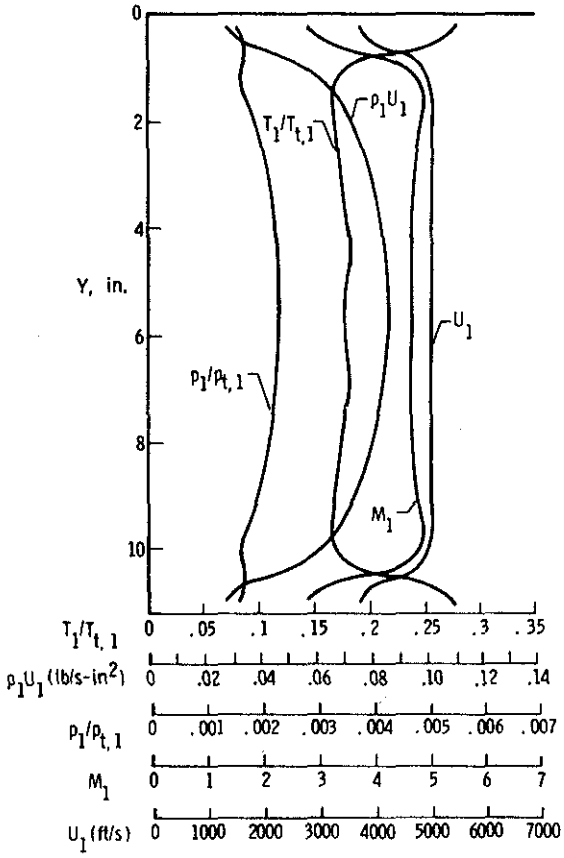

Fig. 11 - Centerline profiles of flow parameters for the Mach 4.7 nozzle (nominal test condition).

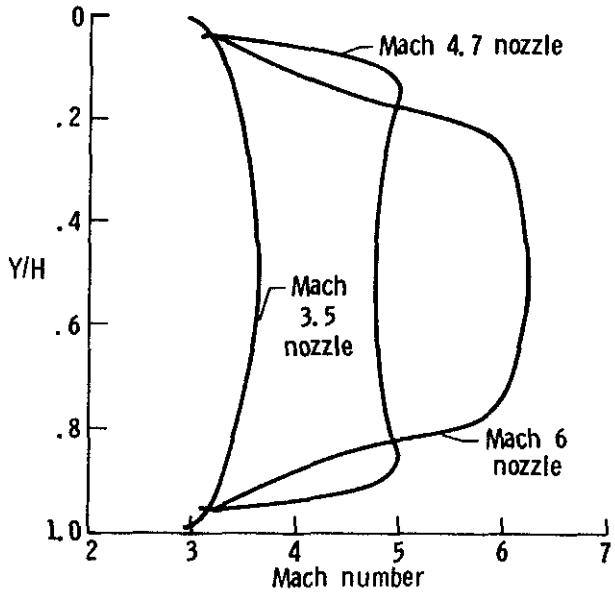

Fig. 12 - Comparison of centerline Mach number profiles for three square cross section contoured nozzles.

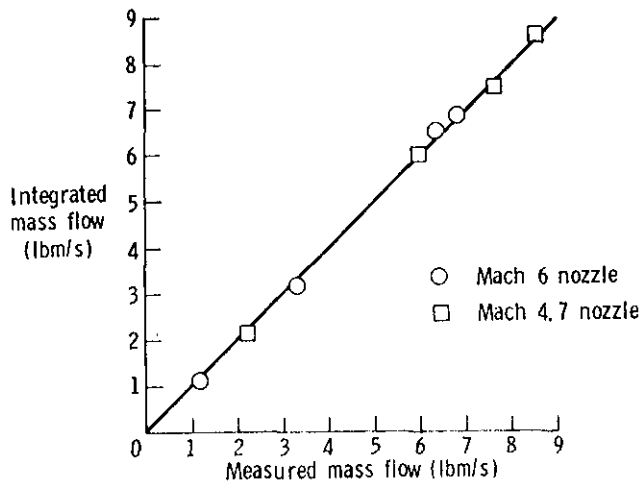

Fig. 13 - Integrated versus measured facility air mass flow rate.

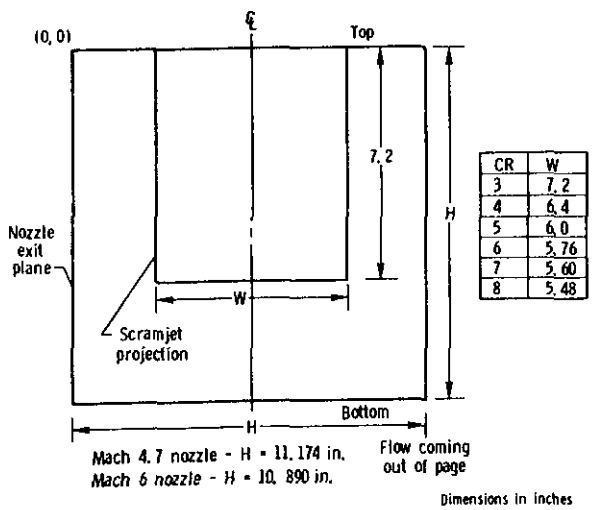

CR	W
3	7.2
4	6.4
5	6.0
6	5.76
7	5.60
8	5.48

Fig. 14 - Projection of the scramjet geometric capture area on the nozzle exit plane.

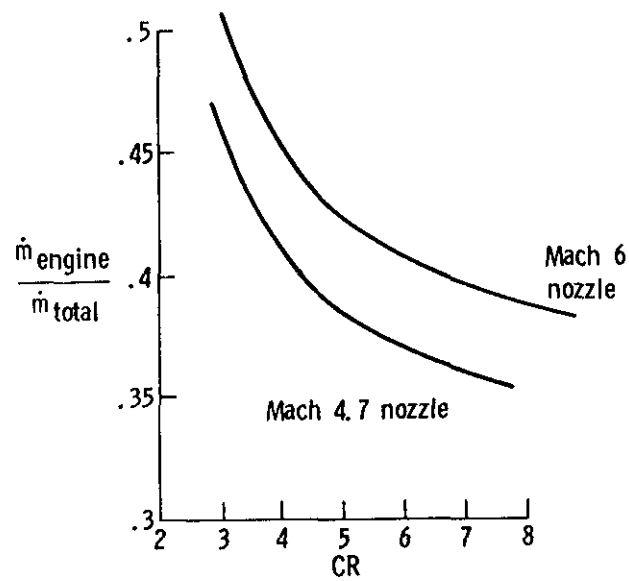

Fig. 15 - Fraction of facility air mass flow rate approaching scramjet engine.